


## Effects of Efimov states on quench dynamics in a three-boson trapped system

A. D. Kerin  and A. M. Martin*School of Physics, University of Melbourne, Parkville, Victoria 3010, Australia*

(Received 15 August 2022; accepted 7 December 2022; published 21 December 2022)

We investigate the effects of Efimov states on the postquench dynamics of a system of three identical bosons with contact interactions in a spherically symmetric three-dimensional harmonic trap. The quench we consider is in the  $s$ -wave contact interaction, and we focus on quenches from the noninteracting to strongly interacting regimes and vice versa. The calculations use the hyperspherical solutions of the three-body problem and enable us to evaluate the semianalytical results of the Ramsey and particle separation, postquench. In the case where the interactions are quenched from the noninteracting to strongly interacting regime we find convergent aperiodic solutions for both the Ramsey signal and the particle separation. In contrast, for quenches from the strongly interacting regime to the noninteracting regime both the Ramsey signal and particle separation are periodic functions. However, in this case we find that the solutions for the particle separation diverge, indicating that in such a system large oscillations may be observable.

DOI: [10.1103/PhysRevA.106.063316](https://doi.org/10.1103/PhysRevA.106.063316)

### I. INTRODUCTION

Efimov states are a unique type of many-body quantum state where short-range interactions create effective long-range forces due to the exchange interaction. They were first predicted by Efimov [1] and first observed by Kraemer *et al.* [2]. Efimov states appear in systems of as few as three bodies [3–9], and while the circumstances under which Efimov states appear is well understood, the specifics of those states, e.g., their energies, can vary depending on the specifics of the system. The influence of Efimov states is highly relevant to a number of topics of cold-gas research, including their effects on, among other quantities, the two- and three-body contacts or three-body decay rates after a quench [10–16].

In this work we consider the dynamics of a system of three identical bosons, interacting via a contact interaction, in an isotropic harmonic trap. Such systems can be constructed in experiment [17–21] in the form of dilute ultracold gases. Specifically, we consider the dynamics of the system after a quench in the contact  $s$ -wave interactions. We consider two quench pathways, from the noninteracting regime to the strongly interacting (unitary) regime and vice versa. We utilize known solutions of the static case [8,9,13,22–24] to calculate the Ramsey signal and particle separation as functions of time following the quench and investigate the effects of different Efimov energy spectra upon the dynamics. Such solutions have been used to calculate thermodynamics quantities such as virial coefficients and Tan contacts [14,21,22,25–37]. In this work we consider a three-dimensional system complementing previous investigations into quench dynamics in two-dimensional [38] and one-dimensional [39–42] systems.

We note that the predictions in this paper are experimentally testable with current techniques. Notably, Ref. [43] prepared a harmonically trapped system of two  ${}^6\text{Li}$  atoms, quenched in *trap geometry* and measured the particle separation.

It is also possible to experimentally obtain systems of three harmonically trapped atoms [17–21], and the quench in  $s$ -wave scattering length is possible using tools such as Feshbach resonance [44–47]. Additionally, experiments measuring the Ramsey signal of trapped cold gases after a quench have been performed [48].

This paper is structured in the following way. Section II provides an overview of the hyperspherical solution to the problem of three identical bosons in a spherical harmonic trap interacting via a contact interaction, including a review of Efimov states. In Sec. III we use the static solutions to calculate observables of the postquench system. We consider the noninteracting to unitary (forwards) and vice versa (backwards) quenches. In these two cases we calculate the Ramsey signal, the overlap of the pre- and postquench states, and the expectation of the particle separation. For the forwards quench we find that both quantities can be calculated semianalytically, and in the reverse case the Ramsey signal is still calculable, but the particle separation diverges.

### II. OVERVIEW OF THE THREE-BODY PROBLEM

To begin, the Hamiltonian of three identical noninteracting bodies in an isotropic three-dimensional harmonic trap is

$$\hat{H} = \sum_{k=1}^3 \left[ \frac{-\hbar^2}{2m} \nabla_k^2 + \frac{m\omega^2 r_k^2}{2} \right], \quad (1)$$

where  $\vec{r}_k$  is the position of the  $k$ th particle,  $m$  is the particle mass, and  $\omega$  is the trapping frequency. For convenience we define the length scales

$$a_\mu = \sqrt{\frac{\hbar}{\mu\omega}}, \quad a_M = \sqrt{\frac{\hbar}{M\omega}}, \quad (2)$$

where  $\mu = m/2$  and  $M = 3m$ .

We use the Bethe-Peierls boundary condition to model the contact interactions [49]

$$\lim_{r_{ij} \rightarrow 0} \left[ \frac{d(r_{ij}\Psi)}{dr_{ij}} \frac{1}{r_{ij}\Psi} \right]_{r_{ij} \rightarrow 0} = \frac{-1}{a_s}, \quad (3)$$

where  $\Psi$  is the total three-body wave function,  $r_{ij} = |\vec{r}_i - \vec{r}_j|$ , and  $a_s$  is the  $s$ -wave scattering length.

The wave function of three identical harmonically trapped atoms subject to Eq. (3) is known [25,50]. In particular the hyperspherical formulation [50] is a closed-form description of the wave function in the strongly interacting (unitary) and noninteracting regimes.

We define the hyperradius  $R$  and hyperangle  $\alpha$  as

$$R^2 = \sqrt{r^2 + \rho^2}, \quad \alpha = \arctan(r/\rho), \quad (4)$$

where

$$\vec{r} = \vec{r}_2 - \vec{r}_1, \quad (5)$$

$$\rho = \frac{2}{\sqrt{3}} \left( \vec{r}_3 - \frac{\vec{r}_1 + \vec{r}_2}{2} \right), \quad (6)$$

and

$$\vec{C} = \frac{\vec{r}_1 + \vec{r}_2 + \vec{r}_3}{3} \quad (7)$$

is the center-of-mass (c.m.) coordinate. The c.m. Hamiltonian is a simple harmonic oscillator (SHO) Hamiltonian. The c.m. wave function is unaffected by Eq. (3) and is a SHO wave function of argument  $\vec{C}$  and length scale  $a_M$ . In hyperspherical coordinates the relative Hamiltonian is given as

$$\begin{aligned} \hat{H}_{\text{rel}} = & \frac{-\hbar^2}{2\mu} \left( \frac{\partial^2}{\partial R^2} + \frac{1}{R^2 \sin(\alpha) \cos(\alpha)} \frac{\partial^2}{\partial \alpha^2} [\cos(\alpha) \sin(\alpha)] \right. \\ & \left. + \frac{5}{R} \frac{\partial}{\partial R} - \frac{4}{R^2} - \frac{\hat{\Lambda}_r^2}{R^2 \sin(\alpha)} - \frac{\hat{\Lambda}_\rho^2}{R^2 \cos(\alpha)} \right) + \frac{\mu\omega^2 R^2}{2}. \end{aligned} \quad (8)$$

We define an ansatz wave function of the form

$$\psi_{3\text{brel}} = N_{qls} \frac{F_{qs}(R)}{R^2} (1 + \hat{P}_{13} + \hat{P}_{23}) \frac{\phi_{ls}(\alpha)}{\sin(2\alpha)} Y_{lm}(\hat{\rho}), \quad (9)$$

where  $N_{qls}$  is the normalization constant,  $F_{qs}$  is the hyperradial wave function, and  $\phi_{ls} = (1 + \hat{P}_{13} + \hat{P}_{23})\phi_{ls}(\alpha)Y_{lm}(\hat{\rho})/\sin(2\alpha)$  is the hyperangular wave function. The exchange operators  $\hat{P}_{13}$  and  $\hat{P}_{23}$  exchange the positions of particles one and three and particles two and three, respectively.

Requiring the ansatz to be an eigenfunction of the Hamiltonian leads to the hyperangular and hyperradial equations

$$s^2 \phi_{ls}(\alpha) = -\phi_{ls}''(\alpha) + \frac{l(l+1)}{\cos^2(\alpha)} \phi_{ls}(\alpha), \quad (10)$$

$$\begin{aligned} E_{\text{rel}} F_{qs}(R) = & \frac{-\hbar^2}{4\mu} \left( F_{qs}''(R) + \frac{F_{qs}'(R)}{R} \right) \\ & + \left( \frac{\hbar^2 s^2}{4\mu R^2} + \mu\omega^2 R^2 \right) F_{qs}(R), \end{aligned} \quad (11)$$

TABLE I. The three-body  $s$  eigenvalues at unitarity for the three-boson case for  $l = 0$  to three decimal places.

$n$	$s$
0	$i \times 1.006 \dots$
1	4.465...
2	6.818...
3	9.324...

and noting that a divergence at  $\alpha = \pi/2$  is nonphysical gives the condition

$$\phi_{ls} \left( \frac{\pi}{2} \right) = 0. \quad (12)$$

Equations (10)–(12) determine the form of  $F_{qs}(R)$  and  $\phi_{ls}(\alpha)$  [26,50,51],

$$F_{qs}(R) = \begin{cases} (\tilde{R})^s e^{-\tilde{R}^2/2} L_q^s(\tilde{R}^2), & s^2 > 0, \\ \frac{1}{\tilde{R}} W_{\frac{E_{\text{rel}}}{2\hbar\omega}, \frac{s}{2}}(\tilde{R}^2), & s^2 < 0, \end{cases} \quad (13)$$

$$\begin{aligned} \phi_{ls}(\alpha) = & \cos^{l+1}(\alpha) \\ & \times {}_2F_1 \left( \frac{l+1-s}{2}, \frac{l+1+s}{2}; l + \frac{3}{2}; \cos^2(\alpha) \right), \end{aligned} \quad (14)$$

where  $L_q^s$  is the associated Laguerre polynomial;  $W_{E_{\text{rel}}/2\hbar\omega, s/2}$  is the Whittaker function;  ${}_2F_1$  is the hypergeometric function;  $\tilde{R} = R/a_\mu$ ,  $q \in \mathbb{Z}_{\geq 0}$ , and  $s^2 \in \mathbb{R}$  are the energy quantum numbers; and  $l \in \mathbb{Z}_{\geq 0}$  is the angular momentum quantum number. In the rest of this work we consider only the  $l = 0$  case for reasons that are elucidated in the Appendix. As such we omit angular momentum indices  $l$  in subsequent notation.

In this framework the  $s$  eigenvalues can be fully specified only in the noninteracting and unitary regime. In the unitary limit applying Eq. (3) to Eq. (9) gives the transcendental equation

$$0 = \left. \frac{d\phi_{ls}'(\alpha)}{d\alpha} \right|_{\alpha=0} + \frac{8}{\sqrt{3}} \phi_{ls} \left( \frac{\pi}{3} \right), \quad (15)$$

which determines the  $s$  eigenvalues; some solutions are presented in Table I. In the noninteracting limit applying Eq. (3) to Eq. (9) gives  $s$  as

$$s = \begin{cases} 2, \\ 2n + 6, \end{cases} \quad (16)$$

for  $l = 0$ , where  $n \in \mathbb{Z}_{\geq 0}$ .

For  $s^2 > 0$ , the universal case, the energy of the wave function is  $E_{\text{rel}} = (2q + s + 1)\hbar\omega$ , which is implicitly determined by Eq. (11) (recall  $q \in \mathbb{Z}_{\geq 0}$ ). For  $s^2 < 0$ , the Efimov case, the energy is not uniquely determined by requiring the wave function, Eq. (9), to be an eigenfunction of the Hamiltonian, Eq. (8); it is, instead, a free parameter. Hence, we require an additional condition to fix the energy. The Efimov hyperradial wave function oscillates increasingly rapidly as  $R \rightarrow 0$ , and we set a condition to fix the phase of the

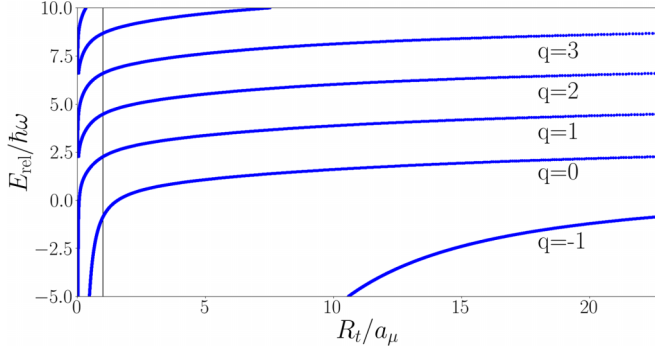


FIG. 1. The energy spectrum for Efimov states as defined by Eq. (17). Calculated using  $s = i \times 1.006 \dots$ . The upper limit on the horizontal axis is  $R_t/a_\mu = e^{\pi/|s|} \approx 22.7$ , and the vertical black line is  $R_t = a_\mu$ .

oscillation [8,50],

$$\arg \Gamma \left[ \frac{1 + s - E_{\text{rel}}/\hbar\omega}{2} \right] = -s \ln \left( \frac{R_t}{a_\mu} \right) + \arg \Gamma(1 + s) \pmod{\pi}, \quad (17)$$

where  $R_t$  is the three-body parameter, an arbitrary parameter with units of distance.  $R_t$  determines the energies of the Efimov states. Physically speaking,  $R_t$  is required because, in the Efimov case, Eq. (11) has an attractive potential term proportional to  $1/R^2$  which allows for arbitrarily small interparticle distances. At small distances the contact interaction assumption breaks down, and the short-range nature of the interaction becomes significant. The Efimov energies are plotted as a function of  $R_t$  in Fig. 1. The energy spectrum is unbounded from below and above; we label the states with  $q \in \mathbb{Z}$ , defining the  $q = 0$  state as the lowest-energy state with  $E_{\text{rel}} > 0$  at  $R_t = \exp(\pi/|s|)a_\mu$ . Note that the energy of the  $q = N$  state evaluated at  $R_t = a_\mu$  is equal to the energy of the  $q = N - 1$  state evaluated at  $R_t = \exp(\pi/|s|)a_\mu$ .

### III. QUENCH DYNAMICS

In this paper we calculate the Ramsey signal and particle separation after a quench in  $a_s$ . As part of this we need to calculate various integrals of the hyperspherical wave function, and their details are presented in the Appendix. The c.m. wave function is unaffected by Eq. (3) and so is unaffected by a quench in  $a_s$ . As such, only the relative motion impacts the system behavior.

The time-dependent postquench relative wave function is given by

$$|\psi(t)\rangle = e^{-i\hat{H}_{\text{rel}}t/\hbar} |F_{q_i s_i} \phi_{s_i}\rangle = \sum_{q,s} \langle F_{q_s} \phi_s | F_{q_i s_i} \phi_{s_i} \rangle e^{-iE_{q_s} t/\hbar} |F_{q_s} \phi_s\rangle, \quad (18)$$

where  $\hat{H}_{\text{rel}}$  is the postquench relative Hamiltonian, quantum numbers with subscript  $i$  refer to the initial state, quantum numbers with no subscripts are the postquench eigenvalues, and  $E_{q_s}$  are the postquench eigenenergies.

#### A. Ramsey signal

The Ramsey signal [48] is defined as the wave-function overlap of the initial and final states,

$$S(t) = \langle \Psi_i(t) | \Psi'(t) \rangle = \sum_{j=0}^{\infty} |\langle \Psi_i(0) | \Psi'_j \rangle|^2 e^{-i(E'_j - E_i)t/\hbar}, \quad (19)$$

where  $\Psi_i$  is the initial state with energy  $E_i$ ,  $\Psi'$  is the postquench state, and  $\Psi'_j$  are the eigenstates of the postquench system with energy  $E'_j$ , where  $j$  sums over all postquench eigenstates.

As mentioned above the c.m. wave function is unaffected by the quench and integrates to 1. Hence, the Ramsey signal depends only on the relative wave function,

$$S(t) = \sum_{q,s} |\langle F_{q_i s_i} \phi_{s_i} | F_{q_s} \phi_s \rangle|^2 e^{-i(E_{q_s} - E_{q_i s_i})t/\hbar}. \quad (20)$$

To evaluate the Ramsey signal we need to evaluate the hyper-radial integral  $\langle F_{q_s} | F_{q_i s_i} \rangle$  and the hyperangular integral  $\langle \phi_s | \phi_{s_i} \rangle$ . The Appendix contains the details of the evaluation of these integrals. With the integrals known, we can then calculate the Ramsey signal for the forwards and backwards quenches. There is a degree of freedom in the choice of the Efimov energy spectrum, determined by the value of  $R_t$ . Whatever the value of  $R_t$  is, the normalization is preserved, but the postquench behavior is, nonetheless, affected by the choice of  $R_t$ .

The Ramsey signal is the weighted sum of oscillators,  $S(t) = Ae^{-iat} + Be^{-ibt} + Ce^{-ict} + \dots$ , where the weights are the square overlaps between the initial state and postquench eigenstates and the angular frequencies are the differences between the initial energy and postquench eigenenergies. The magnitude is similarly a weighted sum of oscillators, but the angular frequencies of the oscillatory terms are the differences between postquench eigenenergies,  $(a - b)$ ,  $(b - c)$ ,  $(a - c)$ ,  $\dots$ . The phase of the Ramsey signal is dominated by the phase of the most heavily weighted terms.

In Fig. 2 we plot the Ramsey signal of the forwards quench for a number of initial states and values of  $R_t$ . The calculations of the Ramsey signal for the forwards quench are performed including only the  $q \geq -1$  Efimov energies, except for the  $R_t = a_\mu$  calculation, which includes only the  $q \geq 0$  Efimov energies. The neglected energies are significantly lower (e.g., for  $R_t = a_\mu$  the  $q = -1$  Efimov energy is  $\approx -566\hbar\omega$ ) and do not contribute meaningfully. Unlike in the two-body case [52] the magnitude of the Ramsey signal of the forwards quench is aperiodic. This is because the postquench eigenenergies are irrational because the unitary  $s$  eigenvalues are irrational, as are the Efimov energies in general. This means the angular frequencies in Eq. (20) ( $a, b, c, \dots$  from the previous paragraph) are irrational, as are the differences between them; hence, the magnitude and phase of the Ramsey signal are aperiodic.

In the  $R_t = a_\mu$ ,  $(q_i, s_i) = (0, 2)$  case (solid red line in the top two panels of Fig. 2) the postquench states with the largest overlaps are  $(E_{q=1}, s) \approx (2.27\hbar\omega, i \times 1.006)$ , with square overlap of  $\approx 0.666$ ;  $(E_{q=0}, s) \approx (-0.85\hbar\omega, i \times 1.006)$ , with square overlap of  $\approx 0.14$ ; and  $(q, s) = (0, 4.465 \dots)$ , with square overlap  $\approx 0.105$ . The two largest modes in the

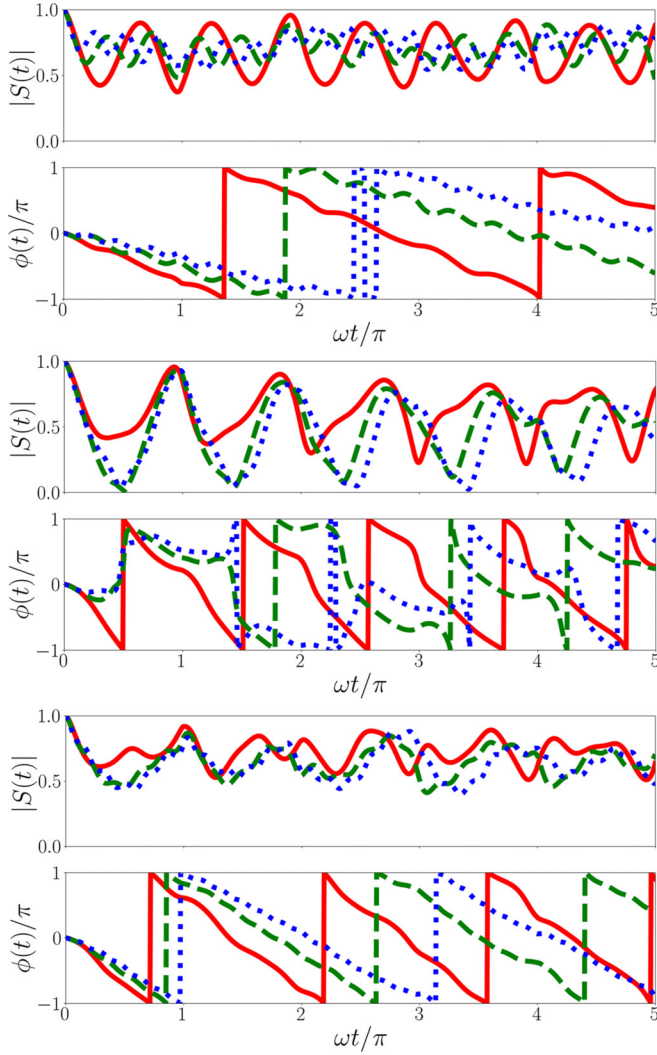


FIG. 2. Ramsey signal of the system quenched from noninteracting to unitarity. In each panel  $s_i = 2$ , the solid red line corresponds to  $q_i = 0$ , the dashed green line corresponds to  $q_i = 1$ , and the dotted blue line corresponds to  $q_i = 2$ . The top two panels use  $R_t = a_\mu$  to calculate the Efimov energy spectrum, the middle panels use  $R_t = 5a_\mu$ , and the bottom panels use  $R_t = 10a_\mu$ . These Ramsey signals are evaluated using Eq. (19) with 40 terms in each of the sums, 1600 terms total. We find that the summation is convergent.

magnitude have periods of  $\approx 2\pi/3\omega$ . The phase is dominated by a period of  $\approx 2.7\pi/\omega$ .

In the  $R_t = 5a_\mu$ ,  $(q_i, s_i) = (0, 2)$  case (solid red line in the middle panels of Fig. 2) the most significant terms are  $(E_{q=0}, s) \approx (1.077\hbar\omega, i \times 1.006)$ , with a square overlap of  $\approx 0.583$ ;  $(E_{q=1}, s) \approx (3.37\hbar\omega, i \times 1.006)$ , with a square overlap of  $\approx 0.24$ ; and  $(q, s) = (0, 4.465, \dots)$ , with a square overlap of  $\approx 0.105$ . The two largest modes in the magnitude have periods of  $\approx 0.87\pi/\omega$  and  $\approx 0.45\pi/\omega$ . The phase is dominated by a period of  $\approx \pi/\omega$ .

In the  $R_t = 10a_\mu$ ,  $(q_i, s_i) = (0, 2)$  case (solid red line in the bottom panels of Fig. 2) the terms with the largest overlaps are  $(E_{q=0}, s) \approx (1.603\hbar\omega, i \times 1.006)$ , with a square overlap of  $\approx 0.72$ ;  $(q, s) = (0, 4.465, \dots)$ , with a square overlap of  $\approx 0.105$ ; and  $(E_{q=1}, s) \approx (3.875\hbar\omega, i \times 1.006)$ , with a square

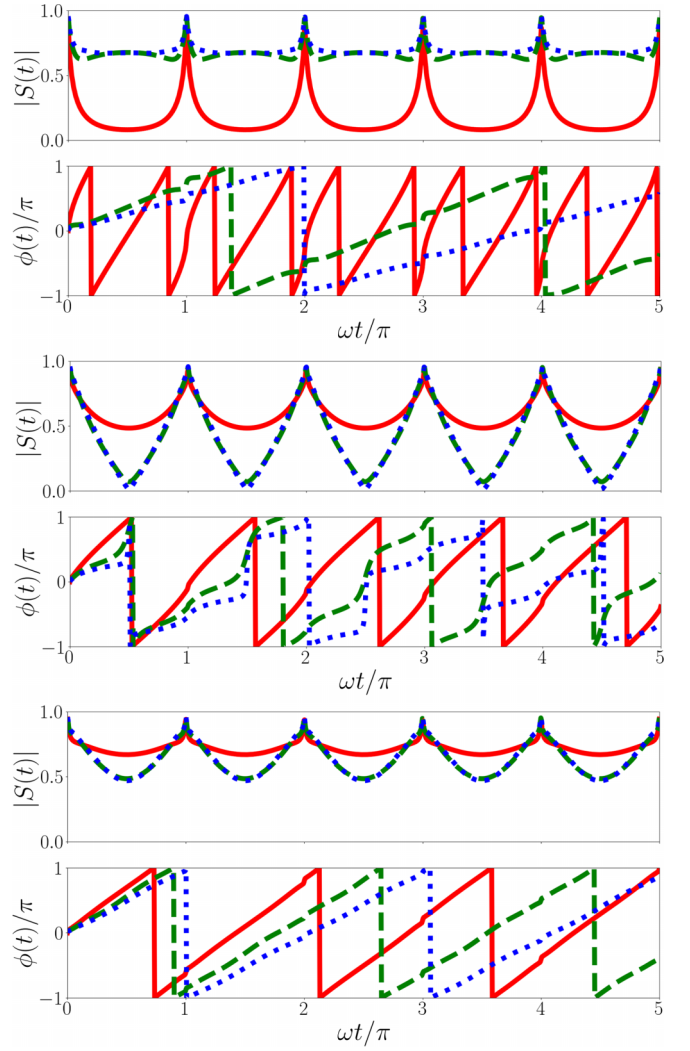


FIG. 3. Ramsey signal of the system quenched from unitarity to noninteracting. In each panel  $s_i = i \times 1.006 \dots$ , the solid red line corresponds to  $q_i = 0$ , the dashed green line corresponds to  $q_i = 1$ , and the dotted blue line corresponds to  $q_i = 2$ . The top two panels use  $R_t = a_\mu$  to calculate the Efimov energy spectrum and thus the energy of the initial state. The middle panels use  $R_t = 5a_\mu$ , and the bottom panels use  $R_t = 10a_\mu$ . These Ramsey signals are evaluated using Eq. (19) with 40 terms in each of the sums, 1600 terms total. We find that the summation is convergent.

overlap of  $\approx 0.092$ . This leads to two main modes in the magnitude with periods of  $\approx 0.5\pi/\omega$  and  $\approx 0.9\pi/\omega$ , and the phase is dominated by a period of  $\approx 1.4\pi/\omega$ .

In Fig. 3 we plot the Ramsey signal of the backwards quench for a system initially in an Efimov state for a variety of Efimov energies. Unlike in the forwards quench the magnitude of the Ramsey signal of the backwards quench is periodic. This is because the noninteracting eigenenergies are all odd-integer multiples of  $\hbar\omega$ . The difference between the postquench eigenenergies is even integers, leading to the magnitude having a period of  $\pi/\omega$ . However, the phase is dominated by the largest term in Eq. (20), and the angular frequencies of each term are irrational because the initial state



is an Efimov state, which, in general, has an irrational energy. This leads to the irregularity in the phase.

For  $R_t = a_\mu$ , ( $E_{q_i=0}, s_i$ )  $\approx (-0.850, i \times 1.006)$  (solid red line in the top panels of Fig. 3) the largest terms are the overlaps with  $(q, s) = (0, 2)$ , with a square overlap of  $\approx 0.14$ , and  $(q, s) = (1, 2)$ , with square overlap of  $\approx 0.12$ . These terms have periods of  $\approx 0.52\pi/\omega$  and  $\approx 0.34\pi/\omega$ . For  $R_t = 5a_\mu$  ( $E_{q_i=0}, s_i$ )  $\approx (1.077, i \times 1.006)$  (solid red line in the middle panels of Fig. 3) the largest term is the overlaps with  $(q, s) = (0, 2)$  with a square overlap of  $\approx 0.58$  and period of  $\approx \pi/\omega$ . For  $R_t = 10a_\mu$  ( $E_{q_i=0}, s_i$ )  $\approx (1.602, i \times 1.006)$  (solid red line in the bottom panels of Fig. 3) the largest term is the overlaps with  $(q, s) = (0, 2)$ , with a square overlap of  $\approx 0.72$  and period of  $\approx 1.43\pi/\omega$ .

### B. Particle separation

We are not limited to calculating only the Ramsey signal. It is also possible to calculate the particle separation  $\langle \tilde{R}(t) \rangle$ .

The expectation value of  $\tilde{R}(t)$  is given as

$$\begin{aligned} \langle \tilde{R}(t) \rangle &= \langle \Psi'(t) | \tilde{R} | \Psi'(t) \rangle = \sum_{j,j'} \langle \Psi_i(0) | \Psi'_j \rangle \langle \Psi'_{j'} | \Psi_i(0) \rangle \\ &\quad \times \langle \Psi'_{j'} | \tilde{R} | \Psi'_j \rangle e^{-i(E_{j'} - E_j)t/\hbar}, \end{aligned} \quad (21)$$

where  $\Psi_i$  is the initial prequench state with energy  $E_i$  and  $\Psi'(t)$  is the postquench state.  $\Psi'_j$  and  $\Psi'_{j'}$  are eigenstates of the postquench system with eigenenergies  $E_j$  and  $E_{j'}$ , respectively, with the sums over  $j$  and  $j'$  taken over all postquench eigenstates.

The c.m. wave function is independent of the interparticle interaction and does not impact the postquench dynamics. Due to the hyperangular wave function's orthogonality in  $s$ , two sums over  $s$  and  $s'$  collapse into a single sum over  $s$ . Hence,  $\langle \tilde{R}(t) \rangle$  is given as

$$\begin{aligned} \langle \tilde{R}(t) \rangle &= \sum_{q,q'} \sum_s \langle F_{q_i s_i} \phi_{s_i} | F_{q' s} \phi_s \rangle \langle F_{q s} \phi_s | F_{q_i s_i} \phi_{s_i} \rangle \\ &\quad \times \langle F_{q' s} \phi_s | \tilde{R} | F_{q s} \phi_s \rangle e^{-i(E_{q s} - E_{q' s})t/\hbar}. \end{aligned} \quad (22)$$

As in Eq. (20), indices with subscript  $i$  refer to the initial state, and indices with no subscript refer to the postquench eigenstates. As for the Ramsey signal all relevant integrals are presented in the Appendix.

In Fig. 4 we plot  $\langle \tilde{R}(t) \rangle$  for a system initially in the noninteracting ground state quenched to unitarity, with the top, middle, and bottom panels corresponding to  $R_t = a_\mu$ ,  $R_t = 5a_\mu$ , and  $R_t = 10a_\mu$ , respectively. For  $R_t \geq 5a_\mu$  we include states with  $q \geq -1$  in the calculations, but for  $R_t = a_\mu$ ,  $E_{q=-1} \approx -566\hbar\omega$ , and this state does not meaningfully contribute, so we include only the  $q \geq 0$  Efimov states in the calculation. In Eq. (22) terms with  $q = q'$  are constants, and the  $s$  contributions to the energies cancel out; the angular frequencies depend only on  $q$  and  $q'$ . The universal-state terms oscillate with an angular frequency that is an even-integer multiple of  $\omega$  because  $q - q'$  is an integer, but the Efimov-state terms oscillate with irrational angular frequencies because the differences between the Efimov energies,  $E_q$  and  $E_{q'}$ , are irrational in general. For each plot we have calculated  $\langle \tilde{R}(t) \rangle$

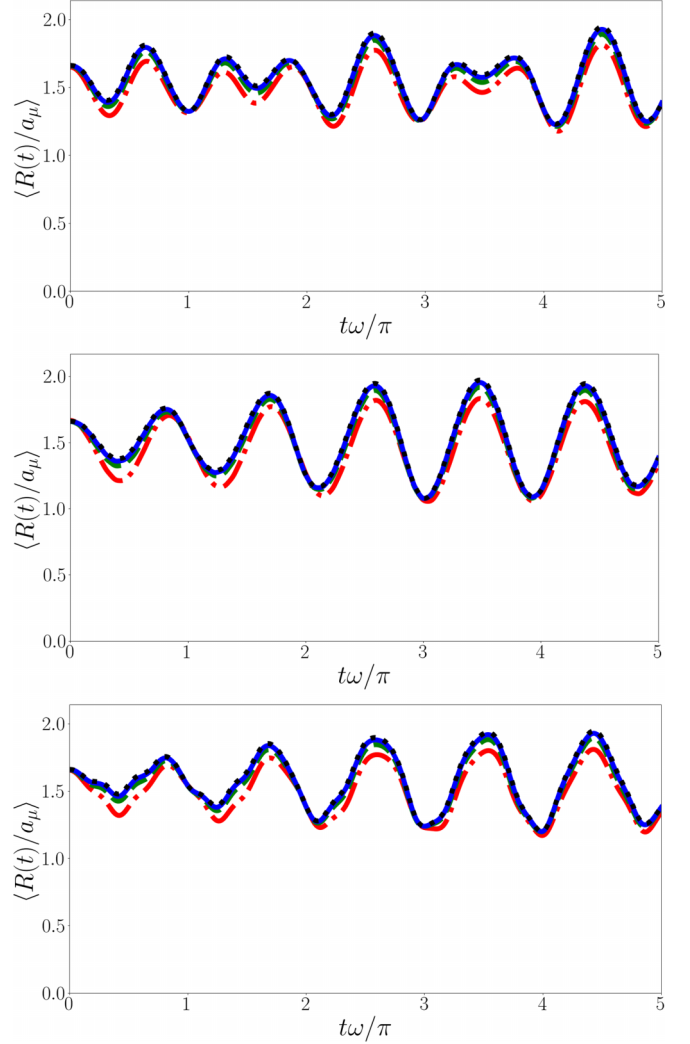


FIG. 4.  $\langle \tilde{R}(t) \rangle$  of a system initially in the ground state quenched from noninteracting to unitarity. The top panel corresponds to  $R_t = a_\mu$ , the middle panel corresponds to  $R_t = 5a_\mu$ , and the bottom panel corresponds to  $R_t = 10a_\mu$ . Efimov states with  $q \geq -1$  are included in the calculation, except  $R_t = a_\mu$ , where  $E_{q=-1} \approx -566\hbar\omega$  does not contribute meaningfully. The dot-dashed red line corresponds to  $N_{\max} = 3$ , the dashed green line corresponds to  $N_{\max} = 6$ , the solid blue line corresponds to  $N_{\max} = 12$ , and the dotted black line corresponds to  $N_{\max} = 24$ . We find that the summation is convergent.

by summing up to  $N_{\max} = 3, 6, 12, 24$  terms in each of the three sums in Eq. (22), and we find that the sum is convergent.

For  $R_t = a_\mu$  the largest oscillating terms are  $(q', q, s) = (q, q', s) = (0, 1, i \times 1.006 \dots)$ , with total coefficient  $\approx 0.17$  and  $E_{q=1} - E_{q=0} \approx 3.12\hbar\omega$ , and  $(q, q', s) = (1, 2, i \times 1.006 \dots)$ , with total coefficient  $\approx 0.09$  and  $E_{q=2} - E_{q=1} \approx 2.12\hbar\omega$ . This implies characteristic periods of  $\approx 2\pi/3\omega$  and  $\approx \pi/\omega$ . For  $R_t = 5a_\mu$  the largest oscillating terms are  $(q, q', s) = (0, 1, i \times 1.006 \dots)$ , with total coefficient  $\approx 0.3$  and  $E_{q=1} - E_{q=0} \approx 2.3\hbar\omega$ , and  $(q, q', s) = (0, 1, 4.465)$ , with total coefficient  $\approx 0.054$  and an associated energy difference of  $2\hbar\omega$ . This leads to characteristic periods of  $\approx 0.9\pi/\omega$  and  $\pi/\omega$ . For  $R_t = 10a_\mu$  the largest oscillating terms are

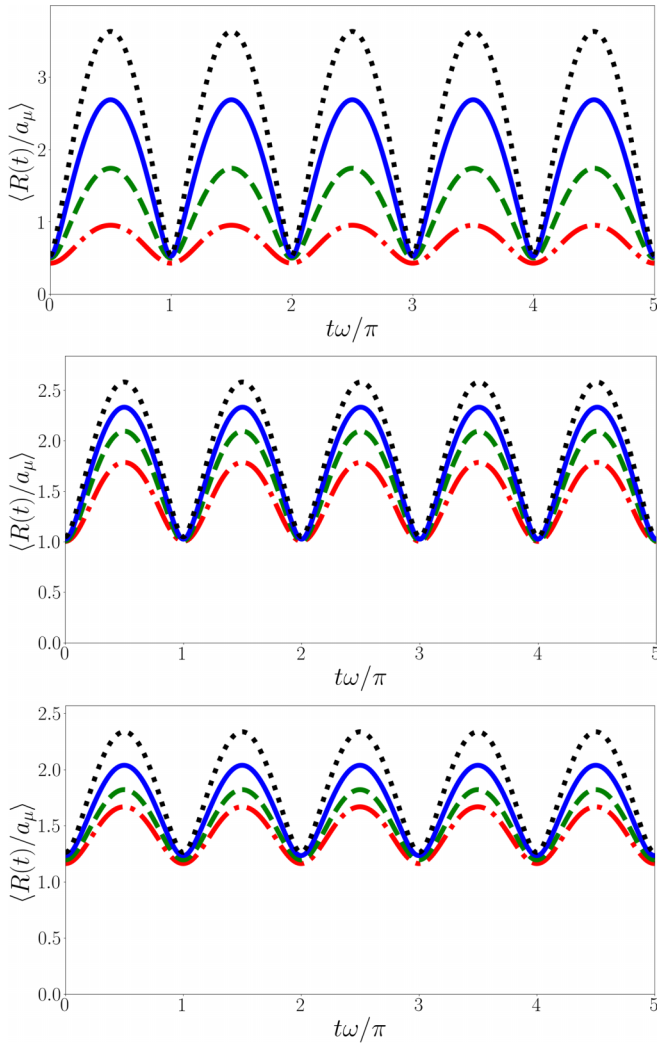


FIG. 5.  $\langle \tilde{R}(t) \rangle$  of a system following a quench from unitarity to noninteracting. The top, middle, and bottom panels correspond to  $R_t = a_\mu$ ,  $R_t = 5a_\mu$ , and  $R_t = 10a_\mu$ , and the corresponding initial states are Efimov states with  $q = 0$ . The dot-dashed red line corresponds to  $N_{\max} = 3$ , the dashed green line corresponds to  $N_{\max} = 6$ , the solid blue line corresponds to  $N_{\max} = 12$ , and the dotted black line corresponds to  $N_{\max} = 24$ .

$(q, q', s) = (0, 1, i \times 1.006 \dots)$ , with total coefficient  $\approx 0.22$  and  $E_{q=1} - E_{q=0} \approx 2.3\hbar\omega$ , and  $(q, q', s) = (0, 1, 4.465)$ , with total coefficient  $\approx 0.054$  and an associated energy difference of  $2\hbar\omega$ . This leads to characteristic periods of  $\approx 0.9\pi/\omega$  and  $\pi/\omega$ .

In Fig. 5 we plot  $\langle \tilde{R}(t) \rangle$  for the backwards quench, where the system is initially in a variety of Efimov states. Unlike the forwards quench we find that  $\langle \tilde{R}(t) \rangle$  is periodic for the backwards quench. This is because in the backwards quench the postquench states are universal states where the differences between eigenenergies are always even multiples of  $\hbar\omega$ , leading to a period of  $\pi/\omega$ . However, similar to how Ref. [52] found a divergence in  $r = |\vec{r}_2 - \vec{r}_1|$  in the backwards quench, we find that  $\langle \tilde{R}(t) \rangle$  also diverges for the backwards quench. In particular we find that it is logarithmically divergent with the number of terms in the summation, i.e.,  $\langle \tilde{R}(t \neq n\pi/\omega) \rangle \propto$

$\ln(N_{\max})$ . This divergence is not exclusively due to the Efimov states as the divergence is present even when there are no Efimov states [53].

This divergence is quite unusual; it is not obvious why it occurs or why it occurs only for the reverse quench. To investigate further we look at how the probability distribution of  $R$ ,  $P(R, t)$ , evolves over time for both quenches.  $P(R, t)$  is given by

$$P(R', t) = \langle \Psi'(t) | \delta(R' - R) | \Psi'(t) \rangle, \quad (23)$$

where  $\Psi'(t)$  is the postquench state.

In Fig. 6 we plot the evolution of  $P(R, t)$  for the forwards quench with  $R_t/a_\mu = 1, 5$ , and  $10$  in the top, middle, and bottom panels, respectively. For all values of  $R_t$  we see a qualitatively similar evolution; the system oscillates between a broad distribution and a tightly peaked one with a smaller mean value. This oscillation is only approximately periodic due to the influence of the irrational Efimov energies. The broad distribution corresponds to the initial universal state, and the tightly peaked distribution is dominated by the Efimov states; the system oscillates between these two regimes.

To understand this oscillation it is useful to consider  $\langle \tilde{R} \rangle$  for the initial and postquench states. For example, for  $R_t = a_\mu$  the states with the largest overlaps with the initial state are  $(E_{q=1}, s) \approx (2.27\hbar\omega, i \times 1.006)$ , with a square overlap of  $\approx 0.666$ , and  $(E_{q=0}, s) \approx (-0.85\hbar\omega, i \times 1.006)$ , with a square overlap of  $\approx 0.14$ ; these states have  $\langle \tilde{R} \rangle \approx 1.5$  and  $\approx 0.57$ , respectively. The initial state is  $(q, s) = (0, 2)$ , so we have  $\langle \tilde{R}(t=0) \rangle \approx 1.66$ ; hence, the position of the initial broad distribution is to the right of the tightly peaked Efimov distribution. As  $R_t$  increases,  $\langle \tilde{R} \rangle$  of the strongly overlapping Efimov states increases, but they are, on average, still less than  $\langle \tilde{R} \rangle$  of the initial universal state; hence, the peak of the narrow distribution moves rightward with increasing  $R_t$ . Additionally, as  $R_t$  increases, the narrow Efimov distribution broadens because the higher-energy Efimov states are simply broader. Note that in the third bottom of Fig. 6 we can see small local peaks in probability near  $\tilde{R} = 0$ . These come from the  $(E_{q=-1}, s) \approx (-5.6, i \times 1.006)$  state and have a square overlap with the initial state of  $\approx 0.01$  and  $\langle \tilde{R} \rangle \approx 0.3$ ; the  $(E_{q=-1}, s)$  state is also accounted for in the  $R_t = 5a_\mu$  calculation, but the overlap is approximately 50 times smaller.

In Fig. 7 we plot  $P(R, t)$  for the backwards quench at  $t = 0, 0.17\pi/\omega, 0.34\pi/\omega$ , and  $\pi/2\omega$ . Unlike the forwards quench the evolution of  $P(R, t)$  here is periodic. The mean of  $P(R, t)$  increases with time, reaching a maximum at  $\pi/2\omega$  before returning to its initial shape at  $t = \pi/\omega$ ; this then repeats with a period of  $\pi/\omega$ . Initially,  $P(R, t)$  is tightly peaked, but it develops a long tail as it evolves, and in Fig. 8 we present the long tail in detail for various values of  $N_{\max}$ . The tail behaves approximately like  $\tilde{R}^{-2}$  until it ends in an exponential-like ‘‘cutoff’’. This cutoff occurs at larger  $R$  for larger  $N_{\max}$ , and in the limit of  $N_{\max} \rightarrow \infty$  the behavior of the tail of  $P(R, t)$  approaches  $\tilde{R}^{-2}$  with no cutoff. This means that the integral of  $P(R, t)$  over  $R$  from  $R = 0$  to  $R \rightarrow \infty$  is finite and properly normalized in the  $N_{\max} \rightarrow \infty$  limit; however,  $RP(R, t)$  has a  $\tilde{R}^{-1}$  tail, and so the integral is not finite, hence the divergence in  $\langle \tilde{R}(t) \rangle$  for the backwards quench.

Physically speaking, there are two likely candidates for the source of the divergence: the zero-range contact interaction

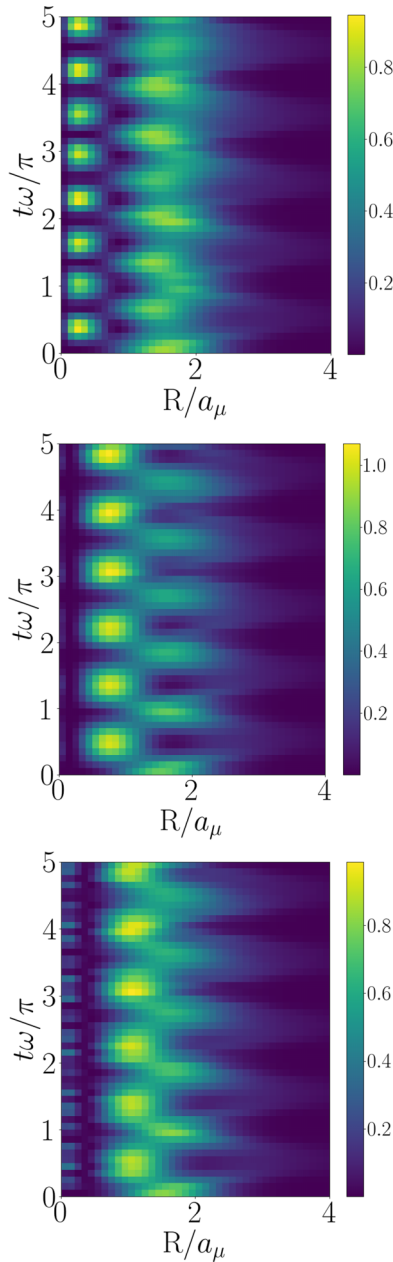


FIG. 6. The evolution of the probability distribution of the hyperradius, Eq. (23), for the forwards quench. The top, middle, and bottom panels correspond to  $R_t/a_\mu = 1, 5,$  and  $10,$  respectively. The horizontal axis is the hyperradius, and the vertical axis is time, with dark blue corresponding to low probability density and yellow corresponding to high density. For all plots the initial state is  $(q_i, s_i) = (0, 2),$  and each plot is constructed with  $N_{\max} = 24.$  In this case  $P(R, t)$  is convergent with  $N_{\max}.$

and the instantaneous nature of the quench; in reality atoms interact at some finite range, and the quench in  $a_s$  occurs over some finite time. These are two nonphysical inputs into this model and may be responsible for the nonphysical outputs.

By considering the finite range of the interaction it is possible to estimate a maximum value of  $\langle \tilde{R}(t) \rangle.$  The length scale of the interaction provides a justification for a maximum energy and thus a cutoff in Eq. (22). Specifically, the range of

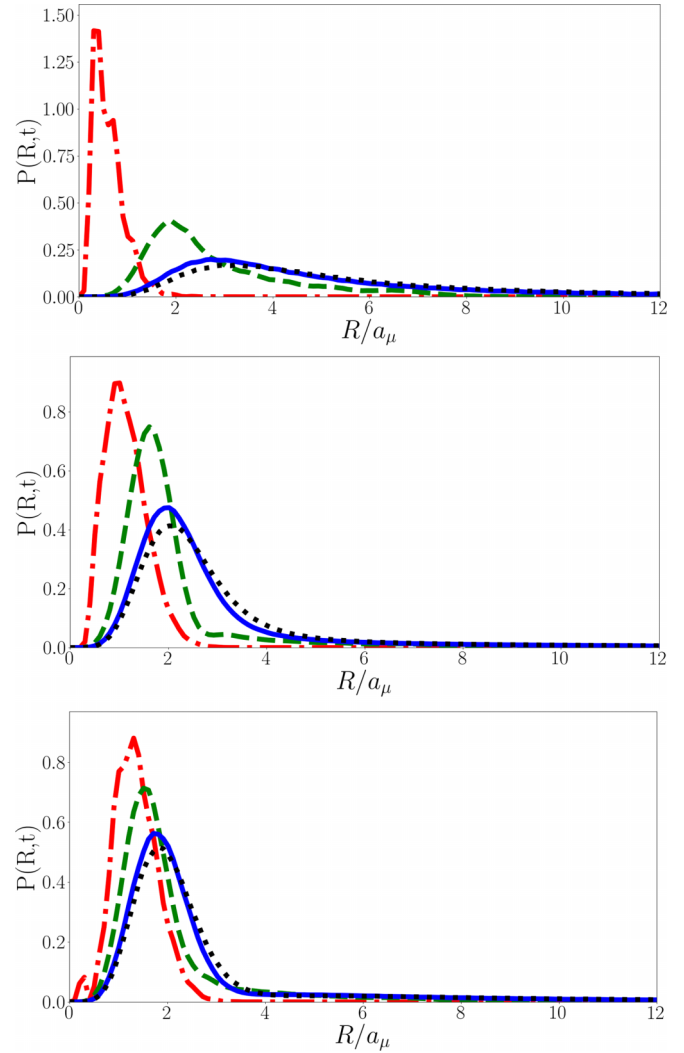


FIG. 7. The evolution of the probability distribution of the hyperradius, Eq. (23), for the backwards quench plotted at  $t = 0$  (dot-dashed red line),  $t = 0.17\pi/\omega$  (dashed green line),  $t = 0.34\pi/\omega$  (solid blue line), and  $t = \pi/\omega$  (dotted black line). The initial states in the top, middle, and bottom panels are the  $q = 0$  Efimov states for  $R_t/a_\mu = 1, 5,$  and  $10,$  respectively. All calculations are performed with  $N_{\max} = 60;$  unlike in the forwards quench, we find that  $P(R, t)$  is convergent only for  $t = 0.$

interaction defines a minimum de Broglie wavelength which defines a maximum energy and thus the cutoff. For sodium in a 1-kHz trap and assuming a van der Waals range of 1 nm, we obtain an energy of  $E_{\text{rel}} \approx 8.7 \times 10^6 \hbar\omega,$  and so we predict  $\langle \tilde{R}(t) \rangle_{\max} \approx 21$  for an initial Efimov energy of  $E_{q=0} \approx -0.85.$  This is an order of magnitude larger than the amplitude of oscillations when the system is quenched from the noninteracting to the strongly interacting regime.

In contrast it is difficult to quantify the effects of a finite-duration quench. In the formalism used here only quenches between the noninteracting and unitary regimes can be described, meaning a quench to or from the intermediate regime cannot be elucidated. However, in the two-body case a quench between any two scattering lengths can be considered [52], so the effects of a finite-duration quench can be investigated.

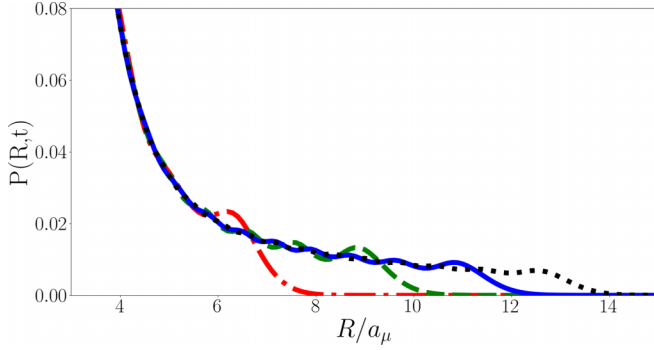


FIG. 8. The tail of  $P(R, t = \pi/2\omega)$  for the reverse quench with the energy of the initial Efimov state given  $E \approx 1.077$  ( $q = 0$  for  $R_t = 5a_\mu$ ) for various values of  $N_{\max}$ . The dot-dashed red line corresponds to  $N_{\max} = 10$ , the dashed green line corresponds to  $N_{\max} = 20$ , the solid blue line corresponds to  $N_{\max} = 30$ , and the dotted black line corresponds to  $N_{\max} = 40$ .

#### IV. CONCLUSION

In this paper we have examined the effects of different Efimov energy spectra on the time-dependent postquench dynamics of an interacting few-body system. This was done in the context of three interacting bosons in a spherically symmetric trap, where the contact interactions were quenched from the noninteracting regime to the strongly interacting regime (forwards quench) and vice versa (backwards quench). In each case we were able to evaluate the postquench dynamics of both the Ramsey signal and the expectation value of the hyperradius.

For the forwards quench we found an irregularly repeating signal for both the Ramsey signal and  $\langle \tilde{R}(t) \rangle$ . For the Ramsey signal this is due to both the Efimov energies and unitary  $s$  eigenspectrum being irrational in general. In the case of the particle separation the contributions from  $s$  cancel out, and the irregularity is due to the irrationality of the Efimov energies. In both cases the results are convergent and well defined.

For the backwards quench the magnitude of the Ramsey signal and  $\langle \tilde{R}(t) \rangle$  oscillate with a period of  $\pi/\omega$ . This is because the noninteracting  $s$  eigenvalues are even integers and Efimov states are not present when  $a_s = 0$ . The phase of the Ramsey signal is still irregular due to the influence of the initial irrational Efimov energy. However, we found, analogous to previous results [52], that the particle separation diverges logarithmically. By enforcing a cutoff on Eq. (22) motivated by a minimum de Broglie wavelength derived from the van der Waals range we expect a maximum  $\langle \tilde{R}(t) \rangle \approx 21$ . This estimate of the size of the oscillations is extremely large compared to the forwards quench case.

#### ACKNOWLEDGMENTS

A.D.K. is supported by an Australian Government Research Training Program Scholarship and by the University of Melbourne. The authors thank V. Colussi for illuminating discussions regarding the evaluation of the hyperangular integral.

#### APPENDIX

In this work we calculate quench observables of systems where the wave functions of the pre- and postquench systems

are known. To obtain these observables we need to perform numerous integrals involving these wave functions. In this Appendix we present those integrals. First, the Jacobian in hyperspherical coordinates is given by

$$dV = d\vec{r}_1 d\vec{r}_2 d\vec{r}_3 = \frac{3\sqrt{3}}{32} R^5 \sin^2(2\alpha) dR d\alpha d\vec{\Omega}_r d\vec{\Omega}_\rho d\vec{C}, \quad (\text{A1})$$

and for convenience we define

$$\langle F_{qs}(R) | F_{q's'}(R) \rangle = \int_0^\infty R F_{qs}(R)^* F_{q's'}(R) dR, \quad (\text{A2})$$

$$\langle \phi_s(\alpha) | \phi_{s'}(\alpha) \rangle = \iint \int_0^{\pi/2} \phi_s(\alpha)^* \phi_{s'}(\alpha) 2 \sin^2(2\alpha) \times d\alpha d\vec{\Omega}_r d\vec{\Omega}_\rho. \quad (\text{A3})$$

To calculate the Ramsey signal, Eq. (20), we need the wave-function overlaps, i.e.,  $\langle F_{qs}(R) | F_{q's'}(R) \rangle$  and  $\langle \phi_s(\alpha) | \phi_{s'}(\alpha) \rangle$ . Whether  $s$  is imaginary or not does not change the functional form of the hyperangular wave function  $\phi_s(\alpha)$ , unlike the hyperradial wave function  $F_{qs}(R)$ . For the hyperangular integral there is only one case, but for the hyperradial integral there are three: the universal-universal, universal-Efimov, and Efimov-Efimov. We begin by considering the hyperangular integral.

The presence of the permutation operators makes evaluating the hyperangular integral directly difficult. To evaluate we transform the permuted terms into the same Jacobi set as the unpermuted term [54]. However, this limits us to the  $l = 0$  case; if the spherical harmonic term is nonconstant, then the coordinate transform is more complicated, and the integral becomes intractable. The hyperangular integral is given by [55–58]

$$\begin{aligned} \langle \phi_{0s} | \phi_{0s_i} \rangle &= 8\pi \int_0^{\pi/2} \left[ (1 + \hat{P}_{23} + \hat{P}_{13}) \frac{\varphi_s(\alpha)}{\sin(2\alpha)} \right]^* \\ &\times \left[ (1 + \hat{P}_{23} + \hat{P}_{13}) \frac{\varphi_{s_i}(\alpha)}{\sin(2\alpha)} \right] \sin^2(2\alpha) d\alpha \\ &= 24\pi \\ &\times \left\{ \int_0^{\pi/2} \varphi_s^*(\alpha) \varphi_{s_i}(\alpha) d\alpha + \frac{4}{\sqrt{3}} \int_0^{\pi/2} \varphi_s^*(\alpha) \right. \\ &\times \left. \left[ \int_{|\pi/3-\alpha|}^{\pi/2-|\pi/6-\alpha|} \varphi_{s_i}(\alpha') d\alpha' \right] d\alpha \right\}. \quad (\text{A4}) \end{aligned}$$

For  $l = 0$  we have [7,56]

$$\varphi_{0s} \propto \sin \left[ s \left( \frac{\pi}{2} - \alpha \right) \right]. \quad (\text{A5})$$

Note that evaluating Eq. (A4) with Eq. (A5) does not give the same result as Ref. [7] in general. This is because Ref. [7] is first concerned with the overlaps with the ground state and, second, combines Eq. (A4) with Eq. (15), so the results presented here and in Ref. [7] agree when  $s$  is a unitary eigenvalue and  $(q_i, s_i) = (0, 2)$ . Note that different hyperangular states of the same regime (i.e., two different unitary values of  $s$  or two different noninteracting values of  $s$ ) are orthogonal, but there is nonzero overlap between unitary and noninteracting states.



The hyperradial integrals are integrals of products of well-understood functions. The universal-universal integral is given by [59]

$$\langle F_{qs}(R) | F_{q_i s_i}(R) \rangle = \frac{a_\mu^2}{2} \binom{q+s}{q} \binom{q_i + \frac{s_i - s}{2} - 1}{q_i} \Gamma\left(\frac{s+s_i}{2} + 1\right) {}_3F_2\left(-q, \frac{s+s_i}{2} + 1, \frac{s-s_i}{2} + 1; s+1, \frac{s-s_i}{2} - q_i + 1; 1\right). \quad (\text{A6})$$

The Efimov-Efimov integral is given by [60]

$$\langle F_{qs}(R) | F_{q_i s_i}(R) \rangle = a_\mu^2 \text{Re} \left[ \frac{\Gamma(s+1)\Gamma(-s)}{\Gamma\left(\frac{1-E_{q_i}/\hbar\omega-s}{2}\right)\Gamma\left(\frac{3-E_q/\hbar\omega+s}{2}\right)} {}_3F_2\left(s+1, 1, \frac{1-E_{q_i}/\hbar\omega+s}{2}; 1+s, \frac{3-E_q/\hbar\omega+s}{2}; 1\right) \right], \quad (\text{A7})$$

and the universal-Efimov integral is given by [60]

$$\begin{aligned} \langle F_{qs}(R) | F_{q_i s_i}(R) \rangle &= \frac{a_\mu^2}{4} \frac{(-1)^{q_i}}{\Gamma(1+q_i)} \left[ \frac{\Gamma\left(\frac{2-s^*+s_i}{2}\right)\Gamma\left(\frac{2+s^*+s_i}{2}\right)\Gamma(-s_i)}{\Gamma(-q_i-s_i)\Gamma\left(\frac{3-E_q/\hbar\omega+s_i}{2}\right)} {}_3F_2\left(1 + \frac{s_i-s^*}{2}, 1 + \frac{s^*+s_i}{2}, -q_i; 1+s_i, \frac{3-E_q/\hbar\omega+s_i}{2}; 1\right) \right. \\ &\quad \left. + \frac{\Gamma\left(\frac{2+s^*-s_i}{2}\right)\Gamma\left(\frac{2-s^*-s_i}{2}\right)\Gamma(s_i)}{\Gamma(-q_i)\Gamma\left(\frac{3-E_q/\hbar\omega-s_i}{2}\right)} {}_3F_2\left(1 + \frac{s^*-s_i}{2}, 1 - \frac{s^*+s_i}{2}, -q_i-s_i; 1-s_i, \frac{3-E_q/\hbar\omega-s_i}{2}; 1\right) \right], \quad (\text{A8}) \end{aligned}$$

where we have used the identity

$$L_n^\alpha(z) = \frac{(-1)^n}{n!} e^{z/2} z^{-(n+1)/2} W_{2n+\alpha+1, \frac{\alpha}{2}}(z). \quad (\text{A9})$$

For the hyperradial integral we find that for  $s = s'$  the integral is zero for  $q \neq q'$ .

To calculate the particle separation expectation value, Eq. (22), we again need to calculate a number of integrals involving the wave function. All the needed integrals except  $\langle F_{q's} | \tilde{R} | F_{qs} \rangle$  are given above. Previously, for the hyperradial integral we had three cases; here we do not need to consider the universal-Efimov case as  $s$  is the same in both the bra and ket due to the orthogonality in  $s$  of the hyperangular integral. For the universal-universal case we have [59]

$$\langle F_{qs}(R) | \tilde{R} | F_{q's}(R) \rangle = \frac{a_\mu^2}{2} \binom{q+s}{q} \binom{q' - \frac{3}{2}}{q'} \Gamma\left(s + \frac{3}{2}\right) {}_3F_2\left(-q, s + \frac{3}{2}, \frac{3}{2}; s+1, \frac{3}{2} - q'; 1\right), \quad (\text{A10})$$

and for the Efimov-Efimov case we have [60]

$$\begin{aligned} \langle F_{qs}(R) | \tilde{R} | F_{q's}(R) \rangle &= a_\mu^2 \text{Re} \left[ \frac{\Gamma\left(\frac{3}{2} + s\right)\Gamma\left(\frac{3}{2}\right)\Gamma(-s)}{\Gamma\left(\frac{1-E_{q'}/\hbar\omega-s}{2}\right)\Gamma\left(\frac{4-E_q/\hbar\omega+s}{2}\right)} \right. \\ &\quad \left. \times {}_3F_2\left(\frac{3}{2} + s, \frac{3}{2}, \frac{1-E_{q'}/\hbar\omega+s}{2}; 1+s, \frac{4-E_q/\hbar\omega+s}{2}; 1\right) \right]. \quad (\text{A11}) \end{aligned}$$

- 
- [1] V. Efimov, *Sov. J. Nucl. Phys.* **12**, 589 (1971).  
[2] T. Kraemer, M. Mark, P. Waldburger, J. G. Danzl, C. Chin, B. Engeser, A. D. Lange, K. Pilch, A. Jaakkola, H.-C. Nägerl, and R. Grimm, *Nature (London)* **440**, 315 (2006).  
[3] O. Kartavtsev and A. Malykh, *J. Phys. B* **40**, 1429 (2007).  
[4] O. Kartavtsev and A. Malykh, *JETP Lett.* **86**, 625 (2008).  
[5] S. Endo, P. Naidon, and M. Ueda, *Few-Body Syst.* **51**, 207 (2011).  
[6] D. S. Petrov, in *Many-Body Physics with Ultracold Gases (Les Houches 2010)*, Lecture Notes of the Les Houches Summer School Vol. 94 (Oxford University Press, Oxford, UK, 2012), p. 109.  
[7] F. Werner, Ph.D. thesis, Université Pierre et Marie Curie Paris VI, 2008.  
[8] S. Jonsell, H. Heiselberg, and C. J. Pethick, *Phys. Rev. Lett.* **89**, 250401 (2002).  
[9] A. Kerin and A. Martin, [arXiv:2204.09205](https://arxiv.org/abs/2204.09205).  
[10] R. J. Fletcher, R. Lopes, J. Man, N. Navon, R. P. Smith, M. W. Zwierlein, and Z. Hadzibabic, *Science* **355**, 377 (2017).  
[11] V. E. Colussi, J. P. Corson, and J. P. D’Incao, *Phys. Rev. Lett.* **120**, 100401 (2018).  
[12] C. Eigen, J. A. Glidden, R. Lopes, E. A. Cornell, R. P. Smith, and Z. Hadzibabic, *Nature (London)* **563**, 221 (2018).  
[13] J. P. D’Incao, J. Wang, and V. E. Colussi, *Phys. Rev. Lett.* **121**, 023401 (2018).  
[14] V. E. Colussi, B. E. van Zwol, J. P. D’Incao, and S. J. J. M. F. Kokkelmans, *Phys. Rev. A* **99**, 043604 (2019).  
[15] S. Musolino, V. E. Colussi, and S. J. J. M. F. Kokkelmans, *Phys. Rev. A* **100**, 013612 (2019).  
[16] S. Musolino, H. Kurkjian, M. Van Regemortel, M. Wouters, S. J. J. M. F. Kokkelmans, and V. E. Colussi, *Phys. Rev. Lett.* **128**, 020401 (2022).  
[17] F. Serwane, G. Zürn, T. Lompe, T. Ottenstein, A. Wenz, and S. Jochim, *Science* **332**, 336 (2011).

- [18] S. Murmann, A. Bergschneider, V. M. Klinkhamer, G. Zürn, T. Lompe, and S. Jochim, *Phys. Rev. Lett.* **114**, 080402 (2015).
- [19] G. Zürn, A. N. Wenz, S. Murmann, A. Bergschneider, T. Lompe, and S. Jochim, *Phys. Rev. Lett.* **111**, 175302 (2013).
- [20] G. Zürn, F. Serwane, T. Lompe, A. N. Wenz, M. G. Ries, J. E. Bohn, and S. Jochim, *Phys. Rev. Lett.* **108**, 075303 (2012).
- [21] T. Stöferle, H. Moritz, K. Günter, M. Köhl, and T. Esslinger, *Phys. Rev. Lett.* **96**, 030401 (2006).
- [22] X. Cui, *Few-Body Syst.* **52**, 65 (2012).
- [23] D. Blume and K. M. Daily, *Phys. Rev. Lett.* **105**, 170403 (2010).
- [24] J. P. Kestner and L.-M. Duan, *Phys. Rev. A* **76**, 033611 (2007).
- [25] X.-J. Liu, H. Hu, and P. D. Drummond, *Phys. Rev. Lett.* **102**, 160401 (2009).
- [26] X.-J. Liu, H. Hu, and P. D. Drummond, *Phys. Rev. A* **82**, 023619 (2010).
- [27] D. Rakshit, K. M. Daily, and D. Blume, *Phys. Rev. A* **85**, 033634 (2012).
- [28] D. B. Kaplan and S. Sun, *Phys. Rev. Lett.* **107**, 030601 (2011).
- [29] B. C. Mulkerin, C. J. Bradly, H. M. Quiney, and A. M. Martin, *Phys. Rev. A* **85**, 053636 (2012).
- [30] B. C. Mulkerin, C. J. Bradly, H. M. Quiney, and A. M. Martin, *Phys. Rev. A* **86**, 053631 (2012).
- [31] S. Nascimbène, N. Navon, F. Jiang, K. Chevy, and C. Salomon, *Nature (London)* **463**, 1057 (2010).
- [32] M. Ku, A. Sommer, L. Cheuk, and M. Zwierlein, *Science* **335**, 563 (2012).
- [33] J. Levinsen, P. Massignan, S. Endo, and M. M. Parish, *J. Phys. B* **50**, 072001 (2017).
- [34] K. M. Daily and D. Blume, *Phys. Rev. A* **81**, 053615 (2010).
- [35] G. Bougas, S. Mistakidis, P. Giannakeas, and P. Schmelcher, *New J. Phys.* **23**, 093022 (2021).
- [36] V. E. Colussi, *Atoms* **7**, 19 (2019).
- [37] T. Enss, N. C. Braatz, and G. Gori, *Phys. Rev. A* **106**, 013308 (2022).
- [38] G. Bougas, S. Mistakidis, P. Giannakeas, and P. Schmelcher, *Phys. Rev. A* **106**, 043323 (2022).
- [39] D. Pęczak, M. Gajda, and T. Sowiński, *New J. Phys.* **18**, 013030 (2016).
- [40] A. G. Volosniev, *Few-Body Syst.* **58**, 54 (2017).
- [41] L. M. A. Kehrberger, V. J. Bolsinger, and P. Schmelcher, *Phys. Rev. A* **97**, 013606 (2018).
- [42] T. Sowiński and M. Á. García-March, *Rep. Prog. Phys.* **82**, 104401 (2019).
- [43] Q. Guan, V. Klinkhamer, R. Klemt, J. H. Becher, A. Bergschneider, P. M. Preiss, S. Jochim, and D. Blume, *Phys. Rev. Lett.* **122**, 083401 (2019).
- [44] U. Fano, *Nuovo Cimento* **12**, 154 (1935).
- [45] H. Feshbach, *Ann. Phys. (NY)* **5**, 357 (1958).
- [46] E. Tiesinga, B. J. Verhaar, and H. T. C. Stoof, *Phys. Rev. A* **47**, 4114 (1993).
- [47] C. Chin, R. Grimm, P. Julienne, and E. Tiesinga, *Rev. Mod. Phys.* **82**, 1225 (2010).
- [48] M. Cetina, M. Jag, R. S. Lous, I. Fritsche, J. T. M. Walraven, R. Grimm, J. Levinsen, M. M. Parish, R. Schmidt, M. Knap, and E. Demler, *Science* **354**, 96 (2016).
- [49] H. Bethe and R. Peierls, *Proc. R. Soc. London, Ser. A* **148**, 146 (1935).
- [50] F. Werner and Y. Castin, *Phys. Rev. Lett.* **97**, 150401 (2006).
- [51] F. Werner and Y. Castin, *Phys. Rev. A* **74**, 053604 (2006).
- [52] A. D. Kerin and A. M. Martin, *Phys. Rev. A* **102**, 023311 (2020).
- [53] A. Kerin and A. Martin, *Phys. Rev. A* **106**, 053310 (2022).
- [54] E. Nielsen, D. V. Fedorov, A. S. Jensen, and E. Garrido, *Phys. Rep.* **347**, 373 (2001).
- [55] D. V. Fedorov and A. S. Jensen, *Phys. Rev. Lett.* **71**, 4103 (1993).
- [56] D. V. Fedorov and A. Jensen, *J. Phys. A* **34**, 6003 (2001).
- [57] E. Braaten and H.-W. Hammer, *Phys. Rep.* **428**, 259 (2006).
- [58] M. Thøgersen, Ph.D. thesis, Universality in Ultra-Cold Few- and Many-Boson Systems, Århus University Denmark, 2009.
- [59] H. M. Srivastava, H. A. Mavromatis, and R. S. Alassar, *Appl. Math. Lett.* **16**, 1131 (2003).
- [60] I. S. Gradshteyn and I. M. Ryzhik, *Table of Integrals, Series, and Products* (Academic Press, Cambridge, MA, 2014).